RESEARCH ARTICLE

INTERNATIONAL RESEARCH JOURNAL OF MULTIDISCIPLINARY TECHNOVATION

Asian Research Association

DOI: 10.54392/irjmt2427

A Novel Approach for Air Quality Index Prognostication using Hybrid Optimization Techniques

Krishnaraj Rajagopal [a,*], Kumar Narayanan [a]

[a] Department of Computer Science and Engineering, Vels Institute of Science, Technology and Advanced Studies, Chennai-600117, Tamil Nadu, India

* Corresponding Author Email: krishnarajonnet@gmail.com

DOI: https://doi.org/10.54392/irjmt2427

Received: 17-12-2023; Revised: 20-01-2024; Accepted: 30-01-2024; Published: 17-02-2024

Abstract: This research presents an innovative deep learning approach for forecasting the Air Quality Index (AQI), a crucial public health concern in both developed and developing countries. The proposed methodology encompasses four stages: (a) Pre-processing, involving data cleaning and transformation; (b) Feature Extraction, capturing central tendency, dispersion, higher order statistics, and Spearman's rank correlation; (c) Feature Selection, using a novel hybrid optimization model, Particle Updated Grey Wolf Optimizer (PUGWO); and (d) an ensembled deep learning model for AQI prediction, integrating a Convolutional Neural Network (CNN), an optimized Bi-directional Long Short-Term Memory (Bi-LSTM), and an Auto-encoder. The CNN and Auto-encoder are trained on the extracted features, and their outputs are fed into the optimized Bi-LSTM for final AQI prediction. Implemented on the PYTHON platform, this model is evaluated through R^2, MAE, and RMSE error metrics. The proposed HRFKNN model demonstrates superior performance with an R-Square of 0.961, RMSE of 11.92, and MAE of 10.29, outperforming traditional models like Logistic Regression, HRFLM, and HRFDT. This underscores its effectiveness in delivering precise and reliable AQI predictions.

Keywords: Air Quality, Prediction, Features, Accuracy, Error Functions, Implementation.

1. Introduction

Numerous nations use the AQI as a benchmark. The atmospheric impurities CO, PM10, NO2, SO2 and O3 are operated for the AQI measurement. These pollutants are present in the air all around the city. The comparison of these six types of air pollutants with the general atmosphere's air quality standards—PM2.5 averaged over 24 hours, PM10 averaged over 24 hours, CO averaged over 8 hours, O3 averaged over 8 hours, NO2 and SO2 on averaged over 1 hour—defines the air quality index. Any pollutant's determined air quality sub-index value will be utilized as the AQI if it has the greatest quantity that day.

There are five different categories for the air quality index criteria: 0-25 AQI extremely excellent, 26-50 AQI good, AQI 51 to hundredth medium, AQI 101 upto 200 began to influence health, and 201 AQI poignant physical condition. The concentration measurements data and level concentration equivalent is familiar with construct types of air contaminant using the equation:

$$P = \frac{P_j - P_i}{(Q_j - Q_i)}(Q - Q_i) + P_i \quad (1)$$

Where the values of Q i and Q j coincide to the range's lowest and highest values, appropriately. P stands for the air quality sub-index value, and Q, P_i, and P_j denote the minimal and uppermost values of the extent with that P assess. Q is a representation of the measurement data's air pollution concentration. Diagrammatic representation of Air Pollutants emission is shown in Figure 1.

Globally, air pollution holds a considerable negative impact on health. According to estimates from the World Health Organization (WHO), in 2012, ambient smogginess is answerable for 3 million premature mortalities yearly worldwide. The WHO European Region, which consists of 53 nations, is projected to have been home to almost 480,000 of those preventable fatalities [1]. Due to their detrimental impact on health, it is crucial to oversee the changeable concentrations of ventilate pollutants in cities aimed to take preventative steps in the future [2]. With a variety of interventions, on several sectorial as well as geographic dimensions, town's air quality may be addressed [3]. A statistic known as the AQI is based on the amount of different grainy case to evaluate the level of smog severity [4]. Humans can anticipate their needs for protection by using AQI. Therefore, precise and timely AQI monitoring is crucial for humans in order to discover effective methods of air pollution mitigation [5].

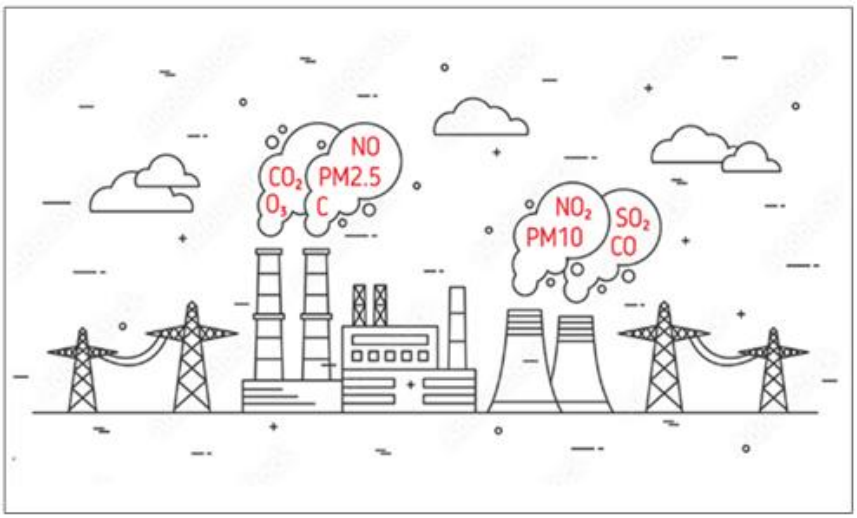

Figure 1. Diagrammatic representation of Air Pollutants emission

The authorities base their calculation of the AQI on the quantity of varied contaminants in the atmosphere, same as small particles and other chemical substances to quantitatively represent the level of air pollution [6]. A higher AQI score, which denotes more severe air pollution, is made by a greater a particular pollutant's composition [7]. Take the use of expensive new commercial detectors or highly precise large established equipment to detect the concentration of a given contaminant [8]. We utilize AQI as an indication for regular assessment of clean look when comes to characterizing air pollution. It demonstrates how clean or filthy the air is and what implications there are for human health. The AQI is calculated for nitrogen dioxide, carbon monoxide and particulate matter (PM) [9, 10]. In most nations, tri toxic gases are most dangerous to human health are suspended solids and ground-level ozone [11].

The two primary kinds of AQI monitoring techniques are monitoring using sensors and monitoring using vision. The sensor-based surveillance systems frequently use detectors observation locations that have been drop in either popular or individual organizations in specific locations throughout a city to track AQI. Due to the great distance between two monitoring sites, this method can only supply coarse-grained 2D control. Large-scale Internet of Things devices is used with fixed stations in cities to accomplish fine-grained AQI surveillance. For AQI monitoring utilizing sensor-based methodologies, mobile devices must collect a specified quantity of air quality data, which necessitates significant energy consumption for moving across vast monitoring regions. Vision-based monitoring techniques include mobile crowdsourcing and static station monitoring, in contrast to sensor-based monitoring strategies [12].

The AQI at restricted locations across the entire region is inferred by static monitoring stations using aerial photographs. Whenever it is risky or challenging to utilise equally human aircraft and ground-level stations, unmanned aerial vehicles (UAVs) with abord sensors to detect emissions of shipping, industrial stack emissions, or emissions from ground vehicles. Therefore, sampling of gaseous pollutants must be done before the UAV's motors mix or scatter the plume in order for UAVs to be successfully used for pollution in air assessment, exceptionally at immobile evasions. The motion of the UAV propellers while they are providing lift causes the air to be bent, which causes the downwash and upwash effect. The crucial step in ensuring accurate sampling is identifying the role that rotor disturbance plays in the transfer of gas to the gas sensors. [13]. The limitations of AQI monitoring include high energy use [14], insufficient monitoring, and privacy issues. Therefore, it is crucial to create a framework that is effective for inspection and estimating AQI values and owns qualities of power save, greater changeability, and secrecy protection [15].

The foremost contribution of the proposed work is as follows,

- To select the optimal features using the new Particle Updated Grey Wolf Optimizer (PUGWO), which is the composite of the standard Particle Swarm Optimization (PSO) and Grey Wolf Optimizer (GWO), respectively.
- To introduce a new ensembled-deep-learning-based-AQI-prediction model that includes the Convolutional Neural Network (CNN), optimized Bi-directional Long Short-Term Memory (Bi-LSTM) and Auto-encoder
- To optimize the weight of Bi-LSTM using the new Particle Updated Grey Wolf Optimizer (PUGWO) model.

The following is how the paper is organized: The most recent research on the suggested system is discussed in section 2. The considered methodology is represented meticulously in 3rd Section. Discussion of

result are covered in Section 4. conclusion is established in Section 5.

2. Literature Review

"Some of the recent research works related to UAV based Air Quality Index were reviewed in this section". Also, Table 1 represents the research gaps in the previously reported work.

Alvear *et. al.,* [16] have proposed a spatial discretization approach and enhanced the solution. One of the most effective mathematical techniques for system optimization was discretization, which changes a continuous domain into its equivalent discrete domain. UAVs can only move within a discretized space's central tile positions., according to the PdUC-Discretized (PdUC-D) enhancement. prevent surveillance investigate the effects of altering the tile size between locations that are close together.

Kalajdjieski *et. a*l., [17] have suggested a novel method for assessing air pollution in specific areas by equating four alternative architectural designs. To improve the classification accuracy, these photos are further augmented through weather information. The suggested method uses generative adversarial circuits and model instruction approaches to talk about the problem of class disparity. According to the studies, the suggested method achieves a reliable accuracy of 0.88., which was equivalent to segment images and traditional models that make use of data on polluted air.

Liu *et. al*., [18] have presented that under restrictions on air quality, a model called MVEMA was already developed to regulate total usage of coal. Machine vision-assisted model (MVA) provides precise measurements online in a potentially hostile environment. without the existence of obtrusive. Air quality restrictions result from the to determine total coal consumption, use the MVA prototype. Air quality, emission regulations, and geographical restrictions are some of the restrictions on air poisoning from lead usage of coal. Based on the MVS, occupational heating systems include options for controlling air pollution as well as economic impacts. Findings demonstrate that under a variety of operating settings, the suggested MVEMA approach for identifying progression situations predicts data quality at 98.33 %.

Villa *et. al*., [19] have proposed Small (UAVs) to monitor air pollution and emissions, as well as to study the atmosphere, such as climate change and to ensure public safety, it is important to use a variety of sensors of the air in industrial and urban settings. The objectives were to gather data of UAVs to study and to evaluate their advantages and scope of use. Three bibliographical databases were used to perform a thorough assessment of the literature, and a total of 60 publications were discovered.

Yang *et. al.,* [20] have proposed the primary air contaminants and the amount of air pollution were identified and assessed by fuzzy comprehensive evaluation. Early warning system's is crucial component was the forecast of air pollutant concentration. Better forecasting could help people make decisions about their work and personal lives. The prediction was extremely difficult, however, due to the complicated and chaotic character of the air pollution statistics themselves. In order to predict the concentration of six important air contaminants, a novel hybrid model was put forth in the research.

Soh *et. al*., [21] have suggested a system to estimate PM2.5 beyond a 48-hour period utilizing data-driven models, ST-DNN. Other contaminants, etc., can all be treated by the suggested procedure. According to the ST-DNN, including a CNN module made first-hour forecasts more accurate because CNN can extract the temporal lag factor from a nearby segmented image by acquisition location data. CNN is also more effective for longer frame predictions.

Mani *et. al*., [22] have presented AQI by the MLR model. After the finding of the association between air pollutants it is verified through the test data that had not yet been observed. For both training and test data, it was determined that performance metrics in addition to ask-fold cross-validationR^2, MAE, and RMSE were sufficient. Second, the portent of AQI was done using the ARIMA model, which has been developed. The ARIMA model was first trained using training data and then tested through test data.

Porag Kalita *et. al*., [23] have presented a 3D AQI chart data Dr-TAPM, mobility tool for operational air pollution surveillance, was effectively used to analyze the data. The factors for air pollution that were taken into account included CO, O_2, particulate matter, and sulphur dioxide.

Zhou *et. al*., [24] have presented two trajectory trace techniques based on a quad-plane arrangement that were investigated and presented to execute 3D air quality policing missions. To achieve that, 3D Boustrophedon pathways were used, and to guarantee the dynamic feasibility, Dubins paths were also used. The circulation forward planner was also advised that, in order an increased coverage rate, the variation in the aforementioned statistic be examined.

Zhang *et. al*., [25] have demonstrated a single-cell cellular connection with many cellphone customers and UAVs, where many UAVs provide information to the base station (BS). It was believed that UAV-to-infrastructure (U2I) and UAV-to UAV (U2U) interactions may support two transmitting modes, notably multi-UAV conversations. In specifically, for the purpose of quality of service, signal-to-noise ratio (SNR) for the U2I network transfers its collected info, but a UAV with a poor SNR to another UAV nearby

Table 1. Research Gaps in the previously reported works

Author	Aim/ Process	Research Gaps
Martinez *et al.* [1]	Health Effects and Economic Costs of Air Pollution	There is no information on whether the WHO air quality guidelines were met.
D. Suprihanto *et al.* [4]	Adults in the US are aware of the Air Quality Index and its effects.	Information on air quality warnings remains unchanged.
Liu *et al.* [5]	Aerial-Ground Air Quality Sensing System	The FL framework is not focused on communication-efficient techniques or novel model compression techniques.
Zhou *et al.* [7]	Using daily data to assess the quality of the air in China	No measurements are made of the amount of air pollution brought on by economic growth using input and output variables.
Villa *et al.* [13]	The creation and testing of a UAV	The development of algorithms for preparing flight paths and ionospheric simulation is not focused.
Alvear *et al.* [16]	UAV-based sensing and a discretized method for monitoring air pollution	Proposed model is not translated to real UAV.
Soh *et. al.* [21]	Predicting Air Quality	Performance is low.
Porag Kalita *et al.* [23]	Low-Altitude Drone Real-Time Air Pollution Monitoring	3D AQI trajectory mapping is not implemented.
Zhou *et al.* [24]	Creating 3D Coverage Paths for Fixed-Wing UAVs	The proposed UAV is not outfitted with a modularized air quality sensor.

by means of underpinning U2U interactions. To permit UAV-to-X contacts, provide a coordinated UAV paradigm. To increase uplink sum rate, we then address the issues with UAV speed optimization and channel allocation.

3. Proposed Methodology

3.1 Overall Architecture Description

In this paper, a novel deep learning method for predicting AQI is contemplated. Figure 2 represents the architecture of the proposed work. The proposed model includes four key steps: (a) Pre-processing, (b) Feature Extraction, (c) Feature Selection and (d) ensembled-deep-learning-based-AQI-prediction. Initially, the collected raw data is pre-processed via data cleaning and data transformation. Then, from the pre-processed data, the features like central tendency (mean and median), “measure of dispersion” (range and standard deviation), higher orrder statistical features (skewness - kurtosis), and Spearman's rank correlation coefficient. Subsequently, from the extracted features, the optimal features are selected through the new hybrid optimization model. The proposed hybrid optimization model (PUGWO) is the combination of the standard PSO and GWO, respectively. Then, using these extracted features, the ensembled-deep-learning-based-AQI-prediction model is trained. This ensembled-deep-learning-based-AQI-prediction includes the CNN, optimized Bi-LSTM and Auto-encoder. The CNN and autoencoder is trained. The outcome is fed as input to the optimized Bi-SLTM. The end outcome with respect to the AQI prediction is acquired from the optimized Bi-LSTM.

3.2 Data preprocessing

Pre-processing is the first step in the proposed model, which involves cleaning and transforming the collected raw data. This step is crucial in ensuring that the data used in the model is accurate and consistent, which can affect the performance of the model. Data cleaning involves removing any irrelevant or missing data, while data transformation involves converting the data into a format that can be used in the model.

3.3 Data cleaning

Repairing or removing wrong, corrupted, inappropriately initialize, replica, or insufficient data from a record is known as data cleaning. Countless opportunities for evidence to be doubled or mistakenly labelled when combining various data feed. Even if consequence and methods show to be rectified, inaccurate data makes them unreliable.

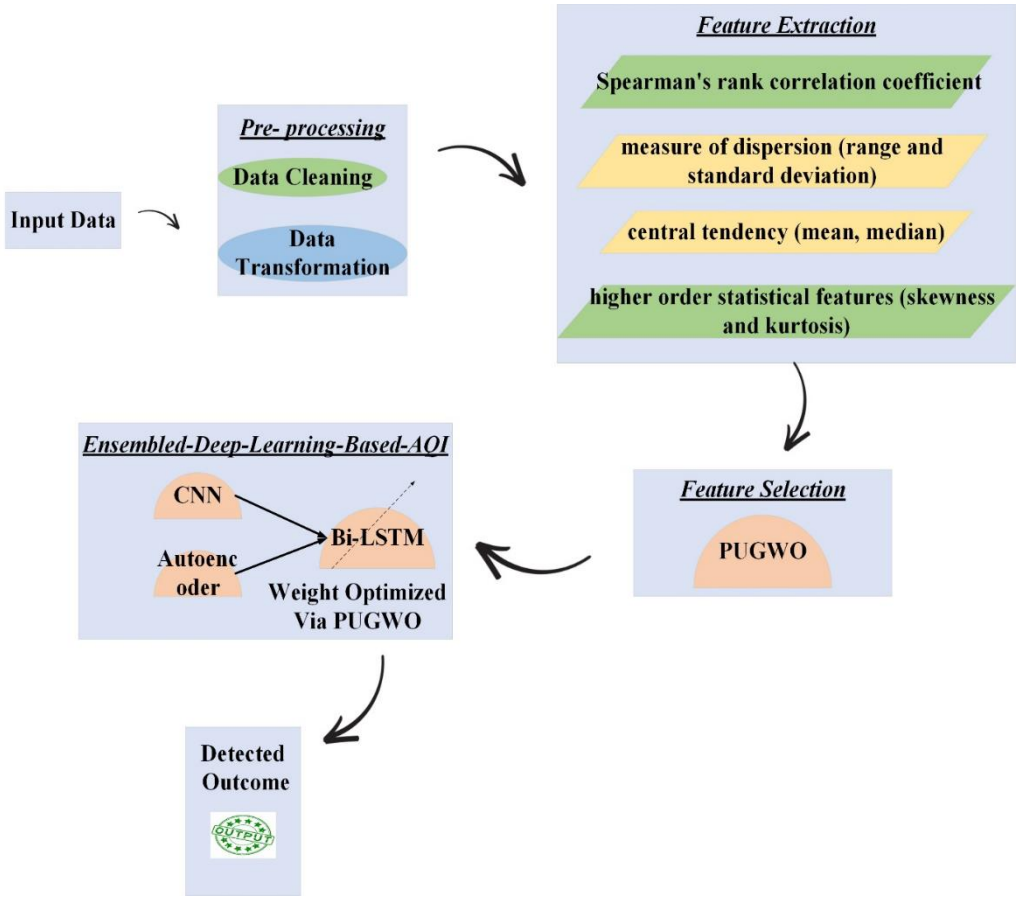

Figure 2. Architecture of the proposed work

accurate steps in the data cleaning process cannot be prescribed in a single, universal way because they differ from dataset to dataset. and do make sure user are carrying out your data cleaning procedure correctly each moment, it is crucial to create a layout.

Having clean data will in the end boost yield and enable you to make decisions based on the best available information. Benefits include:

- Eradication of errors when different data origins are complicated.
- Happy customer and less frustrated personnel result from reduced blunders.
- capacity to organize the miscellaneous functions and the calculated uses of your facts.
- inspection errors and increase reporting to determine the source of flaws,
- construction decisions more immediately and with increased competence will be possible with the use of statistics cleaning apparatus.

3.4 Data Transformation

The operation of transform data from into a format, such as a database file, XML document, into different is known as data transformation. An enterprise data programme must include data transformation because it offers the following advantages:

- higher data quality,
- fewer errors like disappeared ethics
- quicker demands and reclamation times
- without resource usage when manipulating facts
- enhance data organisation and supervision
- more functional evidence, particularly for innovative business intellect or chart.

3.4.1. Examples of Data Transformation

There are many different data turnaround techniques, some of which are as follows:

- Aggregation
- Attribute construction
- Discretization
- Integration
- Manipulation
- Normalization
- Smoothing

3.5. Feature Extraction

Feature extraction involves identifying and extracting relevant information from the pre-processed data. In this case, proposed model extracts visage such as central tendency, measure of dispersion, higher order statistical features, and Spearman's rank correlation coefficient. These features help in capturing the underlying patterns in the data, which are useful in making predictions.

3.5.1. Central Tendency

A central trend measurement is unique evaluate that ventures to delineate a dataset by identifying the central position in that dataset. Thus, central trend measures are sometimes referred to as central location measures. The data are also classified as summary statistics. There are extra estimates of central tendency seems to be maybe the one you are greatest acquainted with.

3.5.1.1 Mean (arithmetic)

The most widely used and recognised indicator of central tendency is the mean. Although both discrete and continuous data can be used with it, continuous variable is the one that is employed most more often. By dividing the number of values in the data set by the number of values in the set, the mean has been calculated. Therefore, if a data set contains n values with values $x1, x2, \ldots, xn$, the sample mean, typically denoted by $\underline{x}$ ("x bar"), is:

$$\underline{x} = \frac{x_1 + x_2 + x_3 \ldots . + x_n}{n} \quad (2)$$

The above formula can also be written as

$$\underline{x} = \frac{\sum x}{n} \quad (3)$$

3.5.1.2. Median

The majority time, the median explains the midpoint of the given group of statistics when it is arranged in a specialised sequence.

Median: Following technique is used when the gathering of data is planned in either upward or downward order:

- If there are an odd number of values or perceptions in the data, the median is unyielding by the $\left[\frac{n+1}{2}\right]$ −th observation.
- If the several values or perceptions in the given data set is even, the median is determined by averaging the $(n/2)$th and $[(n/2)+1]$th observation.

The strategy below can be used to establish the median for dataset,

$$Median = l + \left(\frac{\frac{N}{2} - cf}{f}\right) \times h \quad (4)$$

3.5.2. Measure of Dispersion

The data scatterings are displayed by the measure of dispersion. It provides information about how the data differ from one another and provides insight into how the data are distributed. The dispersion metric reveals whether the distribution of the observations is homogeneous or heterogeneous.

Measures of dispersion should have the following characteristics:

- They should have a strict definition;
- They should be simple to calculate and comprehend;
- Not significantly impacted by variation in comments;
- supported on all comments

3.5.2.1. Classification of Measures of Dispersion

The criterion of dispersion is sorted as:

(i) Thorough criterion of dispersion:

- The measures, such as range and quartile deviation, communicate the scattering of considerations in terms of lengths.
- Using average deviations from comments, such as mean deviation and standard deviation, the measure exhibits variations.

(ii) A proportional evaluate of dispersion:

For comparing the dispensations of two or more collection of data as well as for unit-free comparison, we use a it.

3.5.2.2. Dispersion Measurement Types

The observations and various central tendency metrics being used have an ongoing impact on the dispersion. Examples of dispersion measures include the following:

1. Range
2. Deviation from the median
3. Deviation from the mean

Range

The term "range" describes the spread between a series lower limit and greatest values. Although the range gives us a good idea of how scatter the data are, we still need other estimates of instability to determine how dispersed the data are from central tendency measurements. The most popular and simple way to measure dispersion is with a range. If the two extreme observations are X_{max} and X_{min}, then

$$Range = X_{max} - X_{min} \quad (5)$$

Qualities of Range

- It is the most basic evaluate of dispersion
- Simple to compute
- Simple to comprehend and self-sufficient of origination shift

3.5.1.3. Standard Deviation (SD)

A SD is the optimistic square root between the given values' arithmetic means divided by the squares of those differences. Greek letter sigma is used to represent it, σ. Additionally, it is known as the root mean square deviation. The formula for the SD is

$$\sigma = \left[(\sum_i (y_i - \underline{y}) / n\right]^{\frac{1}{2}} = \left[\left(\frac{\sum_i y_i^2}{n}\right) - \underline{y}^2\right]^{\frac{1}{2}} \quad (6)$$

Specifically, it is for a grouped frequency distribution.

$$\sigma = \left[(\sum_i (y_i - \underline{y}) / N\right]^{\frac{1}{2}} = \left[\left(\frac{\sum_i f_i y_i^2}{n}\right) - \underline{y}^2\right]^{\frac{1}{2}} \quad (7)$$

The variance is equal to the double of the SD. Additionally, it is a dispersion measure.

$$\sigma^2 = \left[(\sum_i (y_i - \underline{y}) / n\right]^{\frac{1}{2}} = \left[\left(\frac{\sum_i y_i^2}{n}\right) - \underline{y}^2\right]^{\frac{1}{2}} \quad (8)$$

for a classified frequency distribution, it is

$$\sigma^2 = \left[(\sum_i (y_i - \underline{y}) / N\right]^{\frac{1}{2}} = \left[\left(\frac{\sum_i f_i y_i^2}{n}\right) - \underline{y}^2\right]^{\frac{1}{2}} \quad (9)$$

3.5.2. Higher order Statistical features (HoS|)

HOS in statistics are functions that use the third or higher power of a sample, as opposed to lower-order statistics' more traditional techniques, that utilize constant, linear, and quadratic terms. first, and second powers)

The two parameters in HOS are Skewness and Kurtosis.

3.5.2.1. Skewness

The degree of asymmetry in our graph is determined by its skewness. When our data deviates from the norm, it is a measure of asymmetry that results. If a data set or distriction appears the same to the left and right of the centre point, it is symmetric.

The skewness formula for univariate dates Y1, Y2,... YN is

$$g_1 = \frac{\sum_{i-1}^{N} (Y_i - \underline{Y})^3 / N}{s^3} \quad (10)$$

Where$\underline{Y}$ is mean, s denotes the SD, and N is no. of marks of data. While in computing the skewness the s is compared with N than N-1.

3.5.2.2 Kurtosis

It serves as a gauge of how heavily or lightly the data deviate from a normal distribution. Alternatively put, data package with a high kurtosis possess heavier tails or outliers Data sets with dejected kurtosis typically lack outliers or have light tails. The baddest screenplay will be a uniform distribution.

$$\text{kurtosis} = \frac{\sum_{i=1}^{N} (Y_i - \underline{Y})^4 / N}{s^4} - 3 \quad (11)$$

By applying this definition, the kurtosis of it with the normal distribution is set to null.

3.5.3. Spearman's Rank Correlation

Spearman's rank correlation estimates the might and guidance of the association amongst two ranked dependent variables. It measures what monotonic a relationship between two variables is, or whether a stepwise function could represent that relationship.

The spearmans rank coefficient formula is

$$\rho = 1 - \frac{6 \sum d_i^2}{n(n^2 - 1)} \quad (12)$$

Where ρ seems to be the Spearmans rank correlation coefficient, di is the contrast amid the two ranks of each assertion, where n is the overall count of inferences.

3.6. Feature selection

Feature selection is operation of choosing important qualities from extracted features. In this case, the proposed model uses the new hybrid optimization model (Particle Updated Grey Wolf Optimizer (PUGWO)) to select the optimal features. The hybrid optimization model combines the standard optimization algorithms to find the best responses. By selecting most important features, the model reduces the dimensionality of the data and improves the performance of the model.

The choice of predictors is crucial because excessively large dimensions of unimportant features can make training take longer, and it must emphasize the value of pricey and time-consuming computation machines. Due to its importance to the outcomes and ability to provide information about feature-related studies and applications, this procedure is crucial. A hybrid PSO-GWO algorithm handles the feature selection step. The benefit of combining the PSO and GWO methods is that, with GWO, the exploration approach is enhanced because the wolves sufficiently explore the search area. The PSO aids in enhancing exploitation so that convergence to the solution and the global optimum can be accomplished promptly. Exploration and exploitation need to coexist in harmony. This improves the performance of both methods when used in conjunction while minimizing the impact of any

drawbacks, such as local stagnation or a suitable convergence speed. By using an inertia weight constant, the changes made to these formulas are to be taken into account. In order for the searching and exploration to be better, the locations of the search agents must first be enhanced. This must oversee the entire process mentioned above.

PSO is an evolutionary computation method that combines population cooperation and competition with individual improvement. A particle's position and velocity determine where it is in space. Position and velocity are the two characteristics that define a particle's status in the search space. In the dimensional search space, the i^{th} particle's position and velocity may be expressed as $a_i = a_1, a_2, a_3, \ldots\ldots, a_n$ and $u_i = u_1, u_2, u_3, \ldots\ldots, u_n$, respectively. Each particle has a best position (pbest) that is $P_i = P_1, P_2, P_3, \ldots\ldots, P_n$ that corresponds to the individual's best objective value at time t. The best particle discovered to date at the time t^* is represented by P_g, which stands for the global best particle (gbest). These calculations are used to determine each particle's new velocity.

$$u_{i,l}(t^* + 1) = yu_{i,l}(t^*) + b_1q_1(P_{i,l} - a_{i,l}(t^*) + b_2q_2(P_{k,l} - a_{i,l}(t^*), \quad \text{l =1, 2, 3, ……., n} \tag{13}$$

The acceleration coefficients constants are represented as b_1 and b_2, the inertia factor is represented as y, Two separate random numbers, q_1 and q_2, are distributed uniformly between 0 and 1. As a result, the following equation determines how each particle's position is generated in each step.

$$a_{i,l}(t^* + 1) = a_{i,l}(t^*) + u_{i,l}(t^* + 1), \text{ l=1, 2, …., n} \tag{14}$$

To prevent particles from excessively roaming outside the search space, each component's value in u_i by Eq. (5) can be defined in the range $[-u_{max}, u_{max}]$. As per Eq. (14), the particle moves in a new direction. Repeating the process until the user-defined stopping criterion is satisfied.

The GWO algorithm's weights are determined by the PSO algorithm, which is as follows. The GWO model weighting parameter combinations are repeatedly optimized using the PSO algorithm until no longer significant fitness increases. In light of this, greater accuracy can be attained when the GWO is used to further upgrade the aforementioned network parameters. We obtain the good combination of parameters when there is a search for these parameters. Similar to the PSO algorithm, the neural network's initial optimization maximises parameters based on the solution, which is then used to enhance network optimization. accuracy and speed.

In order to attain optimization, the GWO algorithm models the wolf leadership hierarchy and predatory behaviour. It then makes use of the abilities of the grey wolf, such as searching for prey, encircling it, hunting, and other predation-related activities.

When N stands for the number of wolves and E for the search area, it is possible to show that $b\,i = b\,1, b\,2, b\,3, \ldots, b\,n$ denotes the location of the ith wolf. Whenever the fittest criterion is fulfilled, the alpha (α) wolf is assumed among the ways to model the social structure of wolves mathematically. The two solutions that come next are known as delta (δ) wolves. beta (β) and Omega (ω) wolves are considered to be the rest of the candidate solutions. According to the algorithm, where the alpha wolf is located corresponds to where the prey is. The following mathematical model can be used to explain how grey wolves circle one another.

$$E = |C^* \times b_v(t) - b(t)| \tag{15}$$

$$b(t + 1) = b_v(t) - A^* \times E \tag{16}$$

The set E is a control coefficient, which is derived from the set t, which is defined by the latest iteration, the set b v (t), which denotes the prey vector location, the set b(t), which represents the grey wolf vector location, and the set b(t).

$$\text{E=}2r_1^* \tag{17}$$

Where the random variable's [0, 1] range is represented by the set r_1^*. According to the following formula, the set A^* is convergence factor is determined.

$$A^* = 2xr_2^* - x \tag{18}$$

$$\text{X=}2(1\text{-}\frac{t'}{T_{max}}) \tag{19}$$

Consider the set r_2^*, which contains random variables with values between [0, 1]. When the x_{max}= 2, x_{min} = 0, the set A^* denotes the control coefficient, and it progressively falls from 2 to 0 throughout the course of iterations. Grey wolves typically instruct the other wolves to surround their victim before they actually take it. The wolf then directs the other wolves as they carry in their victim. The α, β, and δ wolves in the grey wolves that are closest to the prey can be used to determine where the prey is by extrapolating from their positions. The following describes the precise mathematical model:

$$E_\alpha = |C^*{}_1 \times b_\alpha(t') - b(t')| \tag{20}$$

$$E_\beta = \left|C^*{}_2 \times b_\beta(t') - b(t')\right| \tag{21}$$

$$E_\delta = |C^*{}_3 \times b_\delta(t') - b(t')| \tag{22}$$

$$b_1 = b_\alpha - A_1^* \times E_\alpha \tag{23}$$

$$b_2 = b_\beta - A_2^* \times E_\beta \tag{24}$$

$$b_3 = b_\delta - A_3^* \times E_\delta \tag{25}$$

$$b(t' + 1) = \frac{b_1 + b_2 + b_3}{3} \tag{26}$$

$$a_{i,j}(t^* + 1) = a_{i,j}(t^*) + u_{i,j}(t^* + 1), \text{ j=1, 2, …., n} \tag{27}$$

The PSO algorithm is used to replace α, β, ω wolves when their positions change to determine the distance between b(t) and the wolves, which is calculated using the formula (20)-(27).

3.7. Ensembled Deep Learning Based AQI Prediction

Classification is the final step in the proposed model, where the AQI prediction is made. The ensembled-deep-learning-based-AQI-prediction model includes the CNN, optimized Bi-LSTM and Auto-encoder. CNN and autoencoder are trained using the extracted features, and the outcome from both is fed as input to the optimized Bi-SLTM. The final AQI prediction is acquired from the optimized Bi-LSTM. The use of deep learning techniques, such as CNN and LSTM, enables the model to learn and make predictions based on the patterns in the data. The use of an ensemble of dissimilar deep learning method improves performance of model by combining the strengths of each technique.

3.7.1 Convolutional Neural Network

A typical CNN architecture comprises of convolution as well as pooling layers alternated after that with one or even additional fully connected layers. A fully connected layer sometimes modified with an average global pooling layer. Moreover, to numerous mapping functions, regulation units like batch normalization as well as dropout are used to maximize the achievement of CNN. The structure of CNN components is essential when creating different architectures and therefore achieves improved performance.

3.7.1.1 Convolutional layer

The convolutional layer is made up of convolutional kernels, with all neuron acting as kernel. Moreover, if such kernel becomes proportional, the convolution procedure is transformed into an intervention of linkage. Convolutional kernels operate by splitting an image through little portions referred as conductive disciplines. The breaking down of an image into relatively small blocks aids in the extraction of feature motifs. Kernel concatenates with images utilizing particular weight set by expanding the components by the analogous pixel of a receptive field. The operation of convolution is put forth as shown in:

$$g_l^k(r,s) = \sum_c \sum_{a,b} n_c(a,b).h_l^k(p,q) \quad (28)$$

Where, $n_c(a,b)$ represents input image tensor n_c element, then, the turnout aspect map of the convolutional operation k is denoted as $g_l^k(1,1), \ldots, g_l^k(r,s), \ldots., g_l^k(R,S)$

3.7.1.2 Pooling layer

Feature motifs that emerge as an outcome appears at various points. When a feature has been extracted, its precise location is much less essential as long because its estimated position comparative to others is maintained. A fascinating local operation is pooling or down sampling.

$$X_l^k = f_r(g_l^k) \quad (29)$$

The pooling operation is depicted in Eqn (2), where X_l^k signifies the pooled feature-map of the layer l for the kth input feature-map g_l^k. Where, (.) r_f is pooling operation kind.

Equation (29) is pooling operation X_l^k depict the pooled feature-map of l th layer for k th input feature-map k Fl, whereas (.) $p\ g$ establishes the variety of pooling operation. usage of the pooling operation aids in the extraction of a mixture of features that are insensitive to computational shifts and minor distortions. Reducing the dimension of the feature-map to an invariant set of features not just to governs the network's complexity but also aids in improving generalization by maximizing the margin. Pooling formulations of various types like average, vmax, L2, spatial pyramid pooling, overlapping, etc. are employed in CNN.

3.7.1.3 Activation Function

The activation function acts as a shot selection and aids in the discovering layers. The activation function is a decision function that assists in the complex patterns learning. The convolved feature-map's activation function is described in the equation (30).

$$F_l^k = f_x(g_l^k) \quad (30)$$

Where, g_l^k represents the convolution output, that assigns to activation function (.)x_f that combines non-linearity and transformed output F_l^k for l[th] is returned. In the above equation, k Fl is an output of a convolution, which is assigned to activation function (.) a g that adds non-linearity and returns a transformed output F_l^k for l[th] layer.

3.7.1.4 Batch normalization

Batch normalization is employed to resolve issues brought on by functionality' inbuilt correlation coefficients shifts. The inner shift is a modification in hidden unit values distribution that reduces convergence and necessitates cautious parameter initialization. The equation depicts batch normalization for the transformed feature-map g_l^k.

$$M_l^k = \frac{g_l^k - \mu_Y}{\sqrt{\sigma_Y^2 + \varepsilon}} \quad (31)$$

Where, M_l^k represents an averaged attribute map, g_l^k is the information feature-map, μ_Y and σ_Y^2 denotes the feature maps mean and varience for mini batch. For numerical stability, ε is added to avoid division by zero.

3.7.1.5 Dropout

Dropout enhances generality by randomized skipping links with a particular probability. a number of

ties which comprehend a “non-linear relation” in NNs are often co-adapted, resulting in overfitting. The chosen architecture is then regarded as an estimation of all suggested networks.

3.7.1.6 Fully connected layer

The fully connected layer is primarily utilized for categorization at the network's end. It is a global operation, as opposed to pooling and convolution. It collects information from stages of component removal and analyzes output of frequently occurring variations everywhere.

3.7.2 Optimized Bi-directional Long-Short-Term Memory (Bi-LSTM)

3.7.2.1 Basic organization of LSTM

Present era, the LSTM is employed in all sequential design tasks, such as natural language processing, motion detection, and speech recognition. The LSTM block calculation is shown below. In this case, the input within this formula enables the block’s input value, and the input variable is designed to protect in the cell's state.

$$p_q = \sigma(R_p S_q + G_p f_{q-1} + a_p) \quad (32)$$

$$\tilde{\upsilon}_q = tanh\,(R_C S_q + G_p f_{q-1} + a_C) \quad (33)$$

Where, p_q denotes input value, $\tilde{\upsilon}_q$ represents Memory cell’s Candidate value, q depicts time steps, f_q depicts output value and the weight matrices are represented as R, *G, a*.

The forget gate controls the state unit’s weight, and its value is calculated by the following expression:

$$f_q = \sigma(R_f S_q + G_f f_{q-1} + a_f) \quad (34)$$

However, after this equation, the updated memory cell’s new state is determined, as illustrated below.

$$v_q = p_q \times \tilde{\upsilon}_q + f_q \times f_{q-1} \quad (35)$$

The following equation calculate the gate's output on preceding calculation:

$$u_q = \sigma(R_u S_q + G_u f_{q-1} + R_u f_q + a_p \quad (36)$$

Finally, use the formula below to evaluate the cells' final output value.

$$f_q = u_q \times tanh\,(v_q) \quad (37)$$

The output gate, which utilizes sigmoidal nonlinearity, blocks the cell's output. The state unit also functions as an extra unit for the various gating units. These operations enabled each one to recognize that the LSTM architecture's long-term dependencies issue is resolved at a low calculation cost.

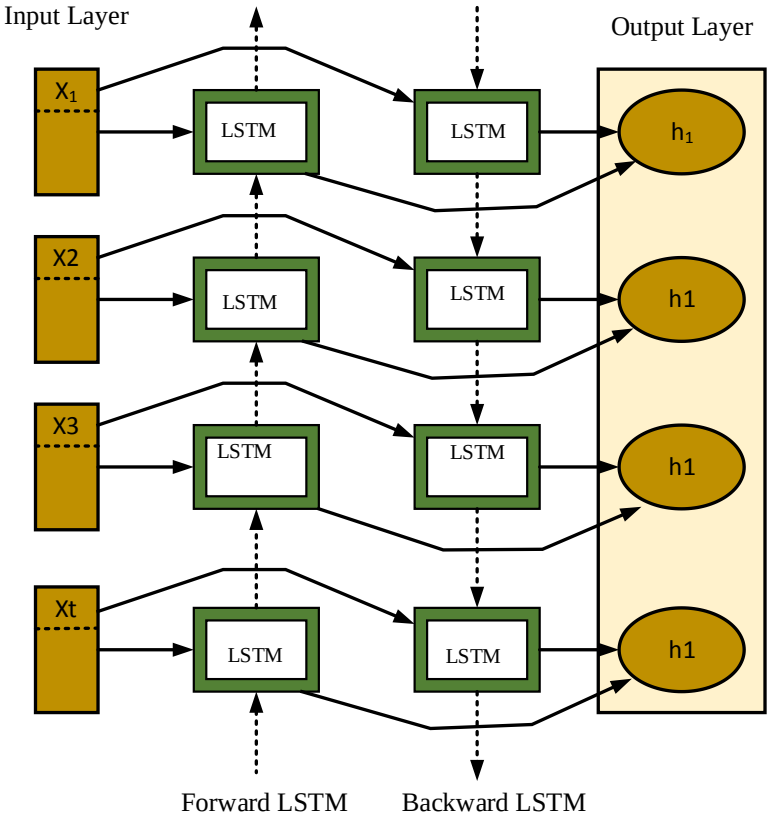

Figure 3. Bi-LSTM

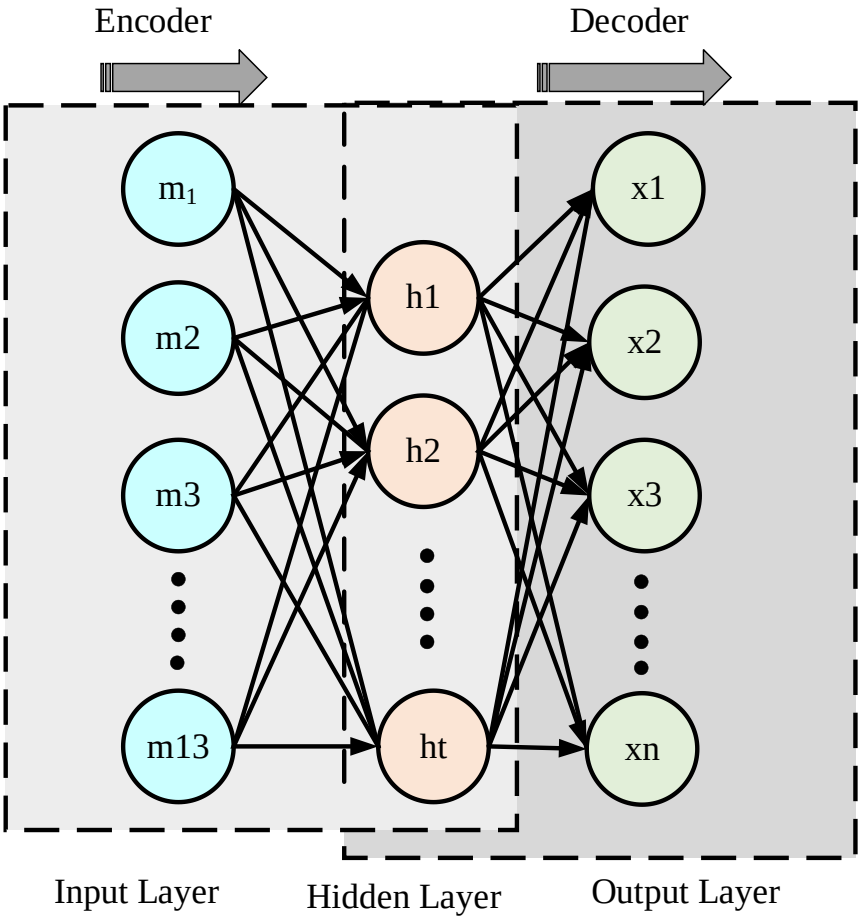

Figure 4. AE Arrangement

3.7.2.2 Bi-LSTM

The Bi-LSTM is made up of LSTM units which work integrating the physical reality from both angles context data. Bi-LSTM learns long-term dependencies while avoiding the retention of redundant context information.

It has shown excellent performance in sequential modelling issues and therefore is broadly utilized text segmentation. The Bi-LSTM network, in contrast to the LSTM network, seems to have 2 parallel layers which propagate in 2 ways with forward as well as reverse passes to gather dependencies in 2 contexts. The scheme of the Bi-LSTM network is shown in Figure 3.

3.7.3 Auto encoder

The set of input features $m(z) = [m_1(z), m_2(z), \dots, m_{13}(z)]$ is denoted as $\tilde{m}(z) = [\tilde{m}_1(z), \tilde{m}_2(z), \dots, \tilde{m}_{13}(z)]$, where $\tilde{m}(k) = m_i(z - f_i)$, and the delay time f_i of the input variables $m_i(z)$.

$$[m_1(z), m_2(z), \dots, m_{13}(z)] = [m_1(z-5), m_2(z-5), \dots, m_{13}(z-6)] \quad (38)$$

Here, AE is employed to minimize data dimensionality, where the no. of hidden layer nodes is lesser than the input layer. The AE structure is shown in Figure 4.

From R_1 (input layer) to R_2 (hidden layer), is an encoding procedure,

$\tilde{m} = [m_1(z-5), m_2(z-5), \dots, m_{13}(z-6)\ ]$ is mapped to R_2 (intermediate hidden layer), and is represented as

$$h = f(wt_1\tilde{m} + bi_1) \quad (39)$$

here, f(.) represents the sigmoid activation function. wt_1 and bi_1 are the encoding stages weight matrix and encoding stages bias vector. Hidden layers output is h. from R_2 to R_1 the R_3 (output layer) is evaluated as follows:

$$x = f(wt_2 h + bi_2) \quad (40)$$

Where, wt_2 is the weight matrix among R_2 and R_3 layers, the offset vector of R_3 is bi_2, the input z values reconstruction is output x, that contains the useful data in z. for loss function the reconstructed error followed is employed:

$$\|x - \tilde{z}\|_2^2 = argmin\ \|f(wt_2 f(wt_1\tilde{z} + bi_1) + bi_2 - \tilde{z}\|_2^2 \quad (41)$$

Where, θ_1, θ_2 are the encoder and decoder parameter set, $\theta_1 = \{wt_1, bi_1\}$, $\theta_2 = \{wt_2, bi_2\}$. In this,

the input dataset's internal non linerar relationship extracts AE, mines the deep feature, and reduce the reconstructed error. Several experiments are presented to evaluate the output neu $x = [x_1(z), x_2(z), \ldots\ldots, x_{10}(z)\ ]$.

4. Result and Discussion

The suggested algorithm was implemented in PYTHON. Among the collected data, 60% of the data was in training purpose, and 40% of the data used for testing purpose.

The graphs are compared with various existing techniques like logistic Regression, Hybrid Random Forest Linear Model (HRFLM) and Hybrid Random Forest Decision Tree (HRFDT). The performance metrics like RMSE, R-square, MAE, MSE and MAPE are used to evaluate the proposed model. The proposed technique is the combination of Recurrent Neural Networks (RNN), CNN and Bi-LSTM.

Dataset-The Pollution Control Division of the Ministry of Natural Resources and Environment produced these conclusions (Air Quality and Noise Management Division, 2020). This research utilizes data from 4 air quality monitoring sites for the months of March through August 2020. Carbon monoxide (CO), Ozone (O3), Sulphur dioxide, Nitrogen dioxide (NO2), and pollutants with an aerodynamic diameter of less than 2.5 m and less than 10 m are all included in this information (SO2).

4.1. Performance comparison

The performance of the prediction model can be assessed using the MAE, RMSE, and R^2 statistics. These parameters can assess the degree of data change and accuracy as well as gauge how well-developed machine learning models predict outcomes. The equation for calculating is

$$MAE = \frac{1}{T}\sum_{i=1}^{T}|a_i - b_i| \quad (42)$$

$$RMSE = \sqrt{\frac{1}{T}\sum_{i=1}^{T}(a_i - b_i)^2} \quad (43)$$

$$R^2 = 1 - \frac{\sum_{i=1}^{T}(a_i - b_i)^2}{\sum_{i=1}^{T}(a_i - \underline{a})^2} \quad (44)$$

4.1. Testing Metrices

4.1.1. Performance Analysis of RMSE

Analysis of RMSE using various existing technique is shown in figure 5. When the training set is 60%, then the value of RMSE for logistic Regression, HRFLM, HRFDT and Ensemble are 31%, 26%, 17% and 13%. When the training set is 70%, then the value of RMSE for logistic Regression, HRFLM, HRFDT and Ensemble are 30%, 26%, 16% and 13%. When the training set is 80%, then the value of RMSE for logistic Regression, HRFLM, HRFDT and Ensemble are 32%,25%,15% and 12%. Compare to existing technique the outcome of the proposed technique is attains low in RMSE.

4.1.2. Performance Analysis of R-Square

Analysis of R-Square using various existing technique is displayed in figure 6. When the training set is 60%, the value of R-Square is recorded for proposed work is 94%, which is better compared to logistic Regression= 81%, HRFLM=84%, HRFDT=87%. When the training set is 70%, the value of R-Square is recorded for proposed work is 95%, which is better compared to logistic Regression= 82%, HRFLM=83%, HRFDT=86%. When the training set is 80%, the value of R-Square is recorded for proposed work is 97%, which is better compared to logistic Regression= 83%, HRFLM=85%, HRFDT=86%.

4.1.3. Performance Analysis of MAE

Investigation of MAE using various existing technique is shown in figure 7. When the training set is 60%, then the value of MAE for logistic Regression, HRFLM, HRFDT and Ensemble are 28%, 23%, 15% and 10%. When the training set is 70%, then the value of MAE for logistic Regression, HRFLM, HRFDT and Ensemble are 27%,22%,16% and11%. When the training set is 80%, then the value of MAE for logistic Regression, HRFLM, HRFDT and Ensemble are 26%,23%,16% and 12%. Compare to existing technique the outcome of the proposed technique is attains low in MAE.

4.1.4. Performance Analysis of MSE

Investigation of MSE using various existing technique is shown in figure 8. When the training set is 60%, the value of MSE is recorded for proposed work is 150, which is better compared to logistic Regression= 950, HRFLM=750, HRFDT=300. When the training set is 70%, the value of MSE is recorded for proposed work is 154, which is better compared to logistic Regression= 951, HRFLM=752, HRFDT=355. When the training set is 80%, the value of MSE is recorded for proposed work is 157, which is better compared to logistic Regression= 970, HRFLM=754, HRFDT=357. The outcome of the proposed is low compared to existing technique.

4.1.5. Performance Analysis of MSE

Examination of MAPE using various existing technique is shown in figure 9. When the training set is 60%, then the value of MAPE for logistic Regression, HRFLM, HRFDT and Ensemble are 30%,27%,17% and 13%. When the training set is 70%, then the value of MAPE for logistic Regression, HRFLM, HRFDT and Ensemble are 29%,26%,16% and 12%. When the training set is 80%, then the value of MAPE for logistic Regression, HRFLM, HRFDT and Ensemble are 32%,24%,15% and 11%. The outcome feature is low compared to existing technique in MAPE.

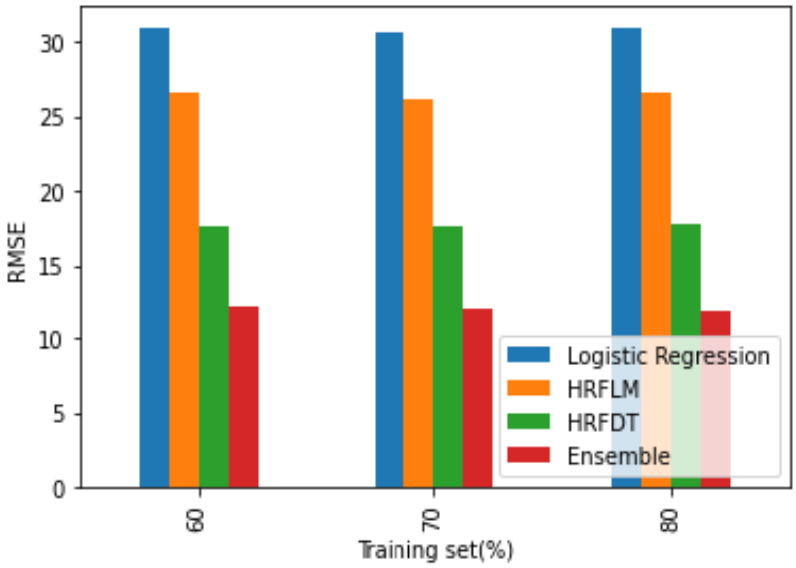

Figure 5. Analysis of RMSE using various existing technique

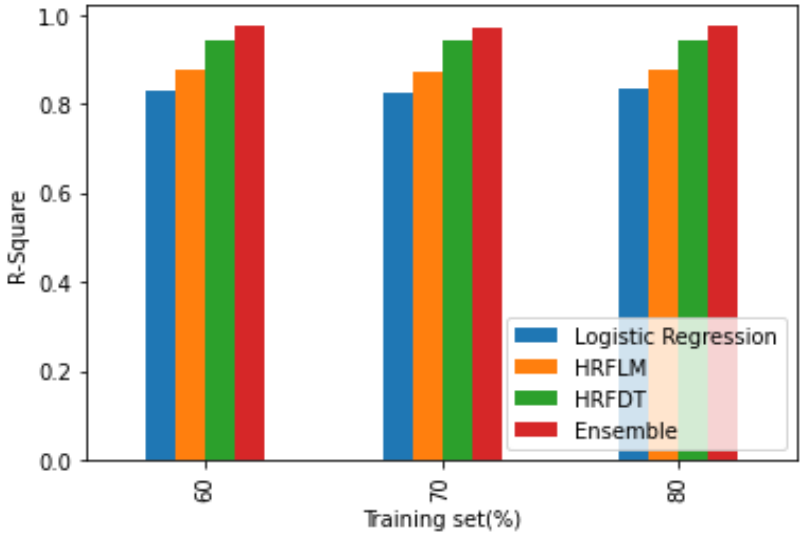

Figure 6. Analysis of R-Square using various existing technique

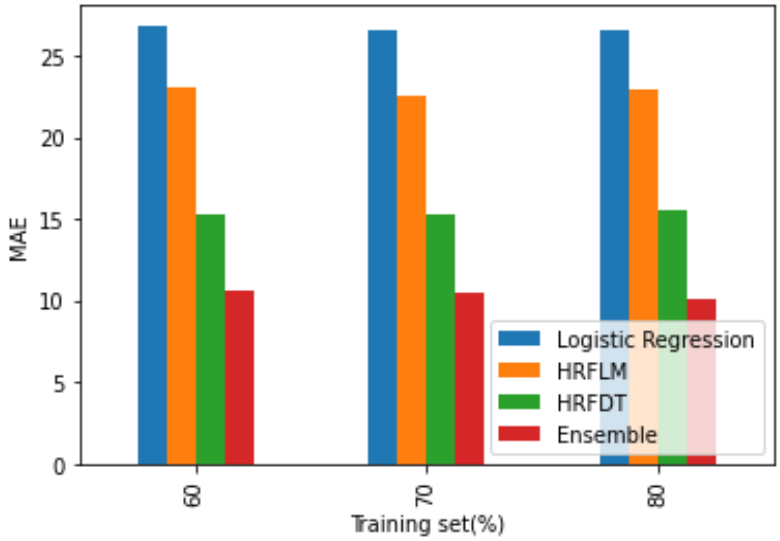

Figure 7. Investigation of MAE using various existing technique

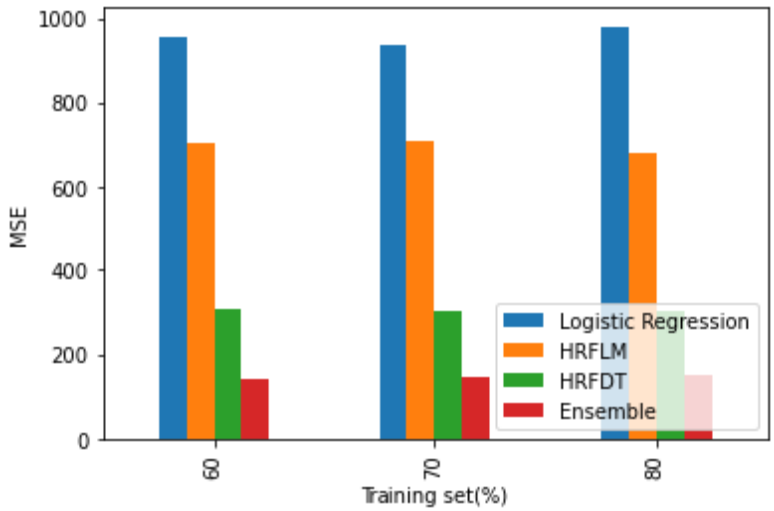

Figure 8. Investigation of MSE using various existing technique

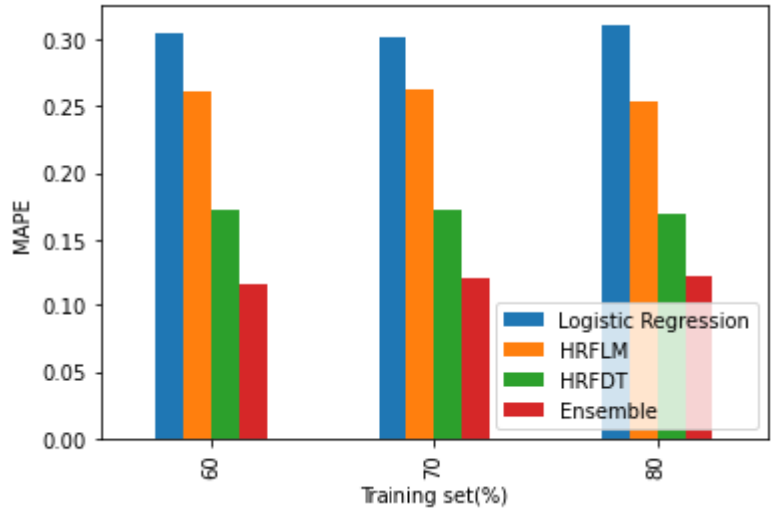

Figure 9. Examination of MAPE using various existing technique

Table 2. Accomplishment of the proposed system

	R-Square	RMSE	MAE
Logistic Regression	0.736138173	31.02099416	26.75141433
HRFLM	0.809081568	26.38708155	22.94112288
HRFDT	0.913890252	17.7212188	15.29359614
HRFKNN	0.96101841	11.92332009	10.29145804

4.2. Overall Performance of Proposed model

Table 2 demonstrate the performance management of the suggested model.

5. Conclusion

In conclusion, a novel deep learning method for predicting the AQI was evaluated in this research. The method consisted by four key steps: Pre-processing, Feature Extraction, Feature Selection, and ensembled-deep-learning-based-AQI-prediction. The raw data was pre-processed and transformed, from which the optimal features were selected using the new hybrid optimization model, PUGWO. The ensembled-deep-learning-based-AQI-prediction model was trained using the extracted features, and included CNN, optimized Bi-LSTM, and Auto-encoder. The performance of the proposed model was evaluated using R^2 coefficient of determination, MAE, and RMSE, and the results showed that the proposed method was effective in predicting AQI with high accuracy. The implementation of the proposed method is been completed utilising the PYTHON platform.

References

[1] G.S. Martinez, J.V. Spadaro, D. Chapizanis, V. Kendrovski, M. Kochubovski, P. Mudu, Health impacts and economic costs of air pollution in the metropolitan area of Skopje. International journal of environmental research and public health, 15(4), (2018) 626. https://doi.org/10.3390/ijerph15040626

[2] P. Kalita, & J. Titabor, OBD-II and oxygen sensor: review the IC engine—emissions related performance. International Journal of Computer Engineering in Research Trends, 3(3), (2016) 98-105.

[3] Z. Sun, D. Zhan, F. Jin, Spatio-temporal characteristics and geographical determinants of air quality in cities at the prefecture level and above in China. Chinese Geographical Science, 29, (2019) 316-324. https://doi.org/10.1007/s11769-019-1031-5

[4] D. Suprihanto, R. Wardoyo, Analysis of classification algorithms for Machine Learning using the SPSS Method. International Journal of Computer Engineering in Research Trends, 10(7), (2023) 15–21.

[5] Y. Liu, J. Nie, X. Li, S.H. Ahmed, W.Y.B. Lim, & C. Miao, Federated learning in the sky: Aerial-ground air quality sensing framework with UAV swarms. IEEE Internet of Things Journal, 8(12), (2020) 9827-9837. https://doi.org/10.1109/JIOT.2020.3021006

[6] Y. Sun, S. Xu, D. Zheng, J. Li, H. Tian, Y. Wang, Effects of haze pollution on microbial community changes and correlation with chemical components in atmospheric particulate matter. Science of the Total Environment, 637, (2018) 507-516. https://doi.org/10.1016/j.scitotenv.2018.04.203

[7] Z. Zhou, X. Guo, H. Wu, J. Yu, Evaluating air quality in China based on daily data: Application of integer data envelopment analysis. Journal of Cleaner Production, 198, (2018) 304-311. https://doi.org/10.1016/j.jclepro.2018.06.180

[8] S. Jaiswal, P. Gupta, Ensemble based Model for Diabetes Prediction and COVID-19 Mortality Risk Assessment in Diabetic Patients. International Journal of Computer Engineering in Research Trends, 10, (2023) 99–106.

[9] H. Amini, N.T.T. Nhung, C. Schindler, M. Yunesian, V. Hosseini, M. Shamsipour, M.S. Hassanvand, Y. Mohammadi, F. Farzadfar, A.M.V. Cabrera, J. Schwartz, S.B. Henderson, N. Künzli, Short-term associations between daily mortality and ambient particulate matter, nitrogen dioxide, and the air quality index in a Middle Eastern megacity. Environmental Pollution, 254, (2019) 113121. https://doi.org/10.1016/j.envpol.2019.113121

[10] I. Suryati, H. Khair, Mapping Air Quality Index of Carbon Monoxide (CO) in Medan City. IOP Conference Series: Materials Science and Engineering, 180(1), (2017) 012114. https://doi.org/10.1088/1757-899X/180/1/012114

[11] B.R. Baddam, D. Shivani, K.S. Reddy, T. Sriya, G. Deepika, Forecasting Air Pollution Concentrations and Binning Air Quality Index Values to Encourage Green Vehicles for Sustainability: A Data Science Approach. International Journal of Computer Engineering in Research Trends, 9(11), (2022) 227–237.

[12] Y. Yang, Z. Zheng, K. Bian, L. Song, Z. Han, Real-time profiling of fine-grained air quality index distribution using UAV sensing. IEEE Internet of Things Journal, 5(1), (2017) 186-198. https://doi.org/10.1109/JIOT.2017.2777820

[13] T.F. Villa, F. Salimi, K. Morton, L. Morawska, F. Gonzalez, Development and validation of a UAV based system for air pollution measurements. Sensors, 16(12), (2016) 2202. https://doi.org/10.3390/s16122202

[14] K. Venkata Ramana, G. Hemanth Kumar Yadav, P. Hussain Basha, L.V. Sambasivarao, Y.V. Balarama Krishna Rao, M. Bhavsingh, Secure and Efficient Energy Trading using Homomorphic Encryption on the Green Trade Platform. International Journal of Intelligent Systems and Applications in Engineering, 12(1s), (2024) 345-360.

[15] R.M. Garland, M. Naidoo, B.A. Sibiya, R. Oosthuizen, (2017). Air quality indicators from the Environmental Performance Index: potential use and limitations in South Africa. Clean Air Journal, 27(1), (2017) 33-41. https://doi.org/10.17159/2410-972X/2017/v27n1a8

[16] O. Alvear, C.T. Calafate, N.R. Zema, E. Natalizio, E. Hernández-Orallo, J.C. Cano, P. Manzoni, A discretized approach to air pollution monitoring using UAV-based sensing. Mobile Networks and Applications, 23, (2018) 1693-1702. https://doi.org/10.1007/s11036-018-1065-4

[17] J. Kalajdjieski, E. Zdravevski, R. Corizzo, P. Lameski, S. Kalajdziski, I.M. Pires, N.M. Garcia, V. Trajkovik, Air pollution prediction with multi-modal data and deep neural networks. Remote Sensing, 12(24), (2020) 4142. https://doi.org/10.3390/rs12244142

[18] Y. Liu, P. Isaev, Simulation of total coal consumption control under air quality constraints

based on machine vision. Soft computing, 25(18), (2021) 12389-12400. https://doi.org/10.1007/s00500-021-05951-7

[19] T.F. Villa, F. Gonzalez, B. Miljievic, Z.D. Ristovski, & L. Morawska, An overview of small-unmanned aerial vehicles for air quality measurements: Present applications and future prospectives. Sensors, 16(7), (2016) 1072. https://doi.org/10.3390/s16071072

[20] P. Kumar, M.K. Gupta, C.R.S. Rao, M. Bhavsingh, & M. Srilakshmi, A Comparative Analysis of Collaborative Filtering Similarity Measurements for Recommendation Systems. International Journal on Recent and Innovation Trends in Computing and Communication, 11(3), (2023) 184-192. https://doi.org/10.17762/ijritcc.v11i3s.6180

[21] P.W. Soh, J.W. Chang, J.W. Huang, Adaptive deep learning-based air quality prediction model using the most relevant spatial-temporal relations. Ieee Access, 6, (2018) 38186-38199. https://doi.org/10.1109/ACCESS.2018.2849820

[22] G. Mani, & J.K. Viswanadhapalli, Prediction and forecasting of air quality index in Chennai using regression and ARIMA time series models. Journal of Engineering Research, 10, (2022) 179-194. https://doi.org/10.36909/jer.10253

[23] P. Kalita, Experimental Study on Automobiles Exhaust Emission Control. International Journal of Computer Engineering in Research Trends, 3(6), (2016) 284–290.

[24] Q. Zhou, L.Y. Lo, B. Jiang, C.W. Chang, C.Y. Wen, C.K. Chen, W. Zhou, Development of fixed-wing UAV 3D coverage paths for urban air quality profiling. Sensors, 22(10), (2022) 3630.https://doi.org/10.3390/s22103630

[25] S. Zhang, H. Zhang, B. Di, L. Song, Cellular UAV-to-X communications: Design and optimization for multi-UAV networks. IEEE Transactions on Wireless Communications, 18(2), (2019) 1346-1359. https://doi.org/10.1109/TWC.2019.2892131

[26] S. Mohan, C. Thirumalai, G. Srivastava, Effective heart disease prediction using hybrid machine learning techniques. IEEE Access, 7, (2019) 81542-81554. https://doi.org/10.1109/ACCESS.2019.2923707

Authors Contribution Statement

Krishnaraj Rajagopal: Conceptualization, Methodology, Data curation, Formal analysis, Validation, Writing – original draft, Writing – review & editing. Kumar Narayanan. Formal analysis, Writing – review & editing. Both the authors read and approved the final version of the manuscript.

Data Availability

For this research, comprehensive data sourced from a Kaggle dataset has been meticulously curated and utilized as the primary foundation for analysis and experimentation.

Has this article screened for similarity?

Yes

About the License